3D simulations of gas puff effects on edge density and ICRF coupling in ASDEX Upgrade

2016 Nucl. Fusion 56 036007

(http://iopscience.iop.org/0029-5515/56/3/036007)

IOP Publishing | International Atomic Energy Agency Nuclear Fusion

Nucl. Fusion **56** (2016) 036007 (11pp) doi:10.1088/0029-5515/56/3/036007

3D simulations of gas puff effects on edge density and ICRF coupling in ASDEX Upgrade

W. Zhang[1,2,3], V. Bobkov[2], T. Lunt[2], J.-M. Noterdaeme[1,2], D. Coster[2], R. Bilato[2], P. Jacquet[4], D. Brida[2], Y. Feng[2], E. Wolfrum[2], L. Guimarais[5] and the ASDEX Upgrade Team[2]

[1] Applied Physics Department, University of Ghent, Ghent, Belgium
[2] Max-Planck-Institut für Plasmaphysik, Garching/Greifswald, Germany
[3] Institute of Plasma Physics, Chinese Academy of Sciences, Hefei, People's Republic of China
[4] CCFE, Culham Science Centre, Abingdon, UK
[5] Instituto de Plasmas e Fusão Nuclear, IST, Universidade de Lisboa, Portugal

E-mail: wei.zhang@ipp.mpg.de

Received 17 September 2015, revised 20 November 2015
Accepted for publication 14 December 2015
Published 5 February 2016

Abstract

In recent experiments, a local gas puff was found to be an effective way to tailor the scrape-off layer (SOL) density and improve the ion cyclotron range of frequency (ICRF) power coupling in tokamaks. In order to quantitatively reproduce these experiments, to understand the corresponding physics and to optimize the gas valve positions and rates, simulations were carried out with the 3D edge plasma transport code EMC3-EIRENE in ASDEX Upgrade. An inter-ELM phase of an H-mode discharge with a moderate gas puff rate (1.2×10^{22} electrons s^{-1}) is used in our simulations. We simulated cases with gas puff in the lower divertor, the outer mid-plane and the top of the machine while keeping other conditions the same. Compared with the lower divertor gas puff, the outer mid-plane gas puff can increase the local density in front of the antennas most effectively, while a toroidally uniform but significantly smaller enhancement is found for the top gas puff. Good agreement between our simulations and experiments is obtained. With further simulations, the mechanisms of SOL density tailoring via local gas puffing and the strategies of gas puff optimization are discussed in the paper.

Keywords: gas puff, ICRF coupling, 3D simulations, plasma edge density

(Some figures may appear in colour only in the online journal)

1. Introduction

Plasma heating in the ion cyclotron range of frequencies (ICRF) is one of the main auxiliary plasma heating methods in tokamaks. It relies on the fast wave (FW) to transport the power from the plasma edge where the antenna is located to the plasma center. Since the FW is evanescent below the cut-off density (typically in the 10^{18} m^{-3} range), the wave decays rapidly in the region where the density is below this value in the scrape-off layer (SOL). The coupling depends strongly on the width of this evanescence region. To a first approximation, the coupled ICRF power can be described by $P_{\mathrm{coupled}} \propto V_{\mathrm{max}}^2 R_{\mathrm{c}}/2Z_{\mathrm{c}}^2$, where V_{max} is the anti-node voltage in the transmission line and Z_{c} is the transmission line characteristic impedance. The coupling resistance R_{c} depends exponentially on the evanescent distance (d_{evan}) between the ICRF antenna and FW cut-off layer, i.e. $R_{\mathrm{c}} \propto R_0 \mathrm{e}^{-\alpha \cdot d_{\mathrm{evan}}}$, where α is the tunneling factor [1]. This evanescence distance can be made smaller by increasing the edge density in front of the ICRF antennas.

Previous experiments in ASDEX Upgrade (AUG) [2, 3], JET [4, 5] and DIII-D [6, 7] show that the edge density can

Table 1. The main parameters of the AUG discharges considered.

		#30634	#30636	#31269	#31273
Gas valve positions	1.3–3.0 s	Lower divertor puff	Lower divertor puff	Lower divertor puff	A13 mid-plane puff
	5.0–7.0 s	A03 mid-plane puff	A02 top puff	A07 top puff	A10 top puff
Common parameters		ELMy H-mode, $H_{98}(y,2) \approx 0.95$			
		Gas puff rate (1.2×10^{22} el s^{-1})			
		$B_t = 2.5$ T, $I_p = 0.8$MA, $P_{total} = 7.8$ MW, $P_{radtot} = 3.2$ MW			
		$P_{ICRF} = 1.5$ MW, $f_{ICRF} = 36.5$MH, $n_{e,cutoff} = 0.4 \times 10^{19}$ m^{-3}			

indeed be increased by using top or outer mid-plane deuterium gas injected close to the antennas instead of divertor gas. An increase by a factor two of antenna loading in these tokamaks was reported for the antennas close to the outer mid-plane valves in [8]. Encouraged by these experiments, maximization of ICRF power by optimizing the gas valve positions and rates is considered in several present and future tokamaks, such as AUG, JET, DIII-D, EAST, WEST and ITER.

In order to quantitatively reproduce the previous experiments, optimize the spatial location of the valves and predict the required amounts of gas, numerical simulations are required. Due to the assumption of toroidal axisymmetry, 2D codes such as EDGE2D-EIRENE cannot quantitatively reproduce the experimental results [8]. In contrast to that, EMC3-Eirene is a coupled Edge Monte Carlo 3D plasma fluid (EMC3) [9] and kinetic neutral particle (Eirene) [10] code. The 3D nature of the code makes it particularly suitable for studying the 3D physics such as gas puff effects on ICRF power coupling. By including the toroidal nonaxisymmetrical Plasma Facing Components (PFCs) and the gas valves at the correct 3D positions, the simulations can be made more realistic. We report the simulation results on an inter-ELM phase of an H-mode discharge with different gas puff locations in AUG. Once the model is validated against experiments, it could be applied to ITER and other future fusion devices in order to predict the optimum gas valve positions and gas puff rate for maximized ICRF power coupling.

In this paper, the simulation setups and validation with experiments are described in section 2. In section 3, the main simulation results are discussed in detail. The mechanisms of how the local gas puff influences the SOL density are presented in section 4. The strategies for optimizing the gas puff are discussed in section 5. Finally conclusions and an outlook are given in section 6.

2. Simulation setups

EMC3-Eirene was originally developed for W7-AS and is now a standard modelling code for helical devices. It has also been widely applied to various tokamaks including ITER [11]. The code is a self-consistently coupled code package of EMC3 [9] and Eirene [10]. EMC3 solves a set of time-independent Braginskii's equations for mass, parallel momentum, electron and ion energy; Eirene is a Monte Carlo solver of Boltzmann equation for neutrals based on the background plasma from EMC3, and provides the source terms to the plasma transport equations in EMC3. Detailed descriptions of the code are referred to [9]. The interest in 3D simulation of the SOL in tokamaks is triggered by the 3D effects of Resonant Magnetic Perturbation (RMP) fields [12, 13], the local gas puff [14] and the 3D particle and energy flow to the main chamber wall [15]. This paper will discuss in detail the implemention of the code in the gas puff studies.

The AUG discharges (table 1) in our study are type-I ELMy H-modes with $B_t = 2.5$ T, $I_p = 0.8$MA, $P_{total} = 7.8$ MW ($P_{ICRF} = 1.5$ MW at 36.5MH) and total radiated power $P_{radiated} = 3.2$ MW. The deuterium gas puff rate in the time periods [1.3, 3.0s] and [5.0, 7.0s] for all discharges are the same (1.2×10^{22} el s^{-1}). Different gas puff methods are investigated in these discharges.

To carry out comprehensive simulations with EMC3-Eirene, a computation grid covering 360° was built and implemented in our simulations. The equilibrium, calculated by CLISTE [16], is from discharge 31269 at 2.1s. Figure 1 illustrates the poloidal cross-section of the computation grid at $\Phi = 11.25°$. Both EMC3 and Eirene share the same grid including the outer core (in red color), the Scrape-Off Layer (SOL) (in blue and green color) and the Private Flux Region (PFR) (in cyan color). The SOL region of the computation grid is extended to the main chamber wall with a part (in green color) which does not necessarily have to be flux surface aligned. The region inside the vessel and outside the SOL (in yellow color) is used only by Eirene. Figure 2 shows the 3D structure of the grid on a flux surface in the SOL. The full 360° grid is composed of sixteen equally constructed segments. Each segment has a toroidal angle of 22.5° and represents a sector in AUG. The PFCs in our computation model include the upper and lower divertors, the inner heat shield, four auxiliary limiters and eight ICRF antenna limiters. For the convenience of calculations, the toroidal angle is counted from −180° to 180°, and the 0° position is chosen at the boundaries of sector 5 and sector 6 (figure 3). In our simulations no impurities are considered, hence the radiated power is subtracted from the total power to approximate the total power deposited on the PFCs by the plasma. The separatrix electron density is about 2.5×10^{19} m^{-3} and is used as a boundary condition in EMC3-Eirene. The gas puff rate (1.2×10^{22} el s^{-1}) in the code was set to be equal to 6% of the total recycling flux, and the rest 94% is treated as the amount of the recyling flux from the main chamber wall and the divertors. By this setting the total particles in our model are kept balanced, and no gas pump was considered in these simulations.

An ELMy H-mode plasmas (#31269 at 2.1s) with lower divertor gas puff rate 1.2×10^{22} el s^{-1} was firstly simulated.

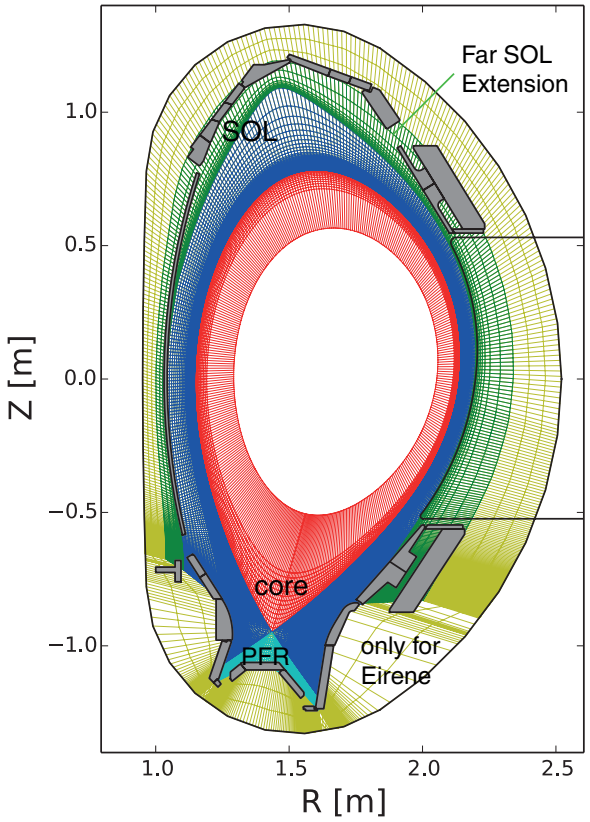

Figure 1. Poloidal cross-section of the computation grid at $\Phi = 11.25°$. The SOL region (in blue and green color) of the grid is extended to the main chamber wall. The plasma facing components include the lower and upper divertors, the inner hear shield and sixteen limiters.

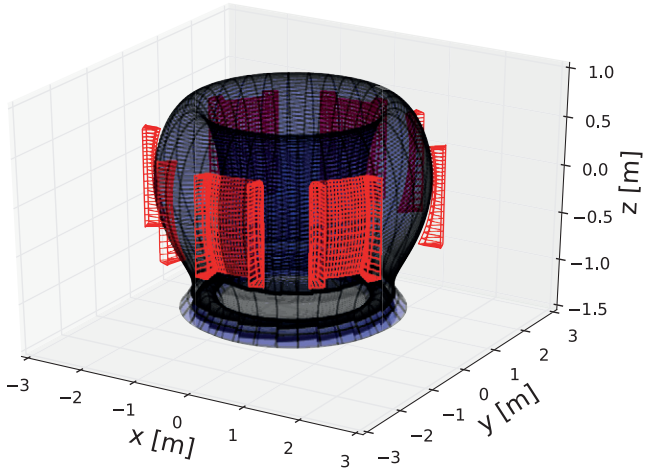

Figure 2. The 3D grid with 8 limiters (two on both sides of each ICRF antenna) and 4 auxiliary limiters.

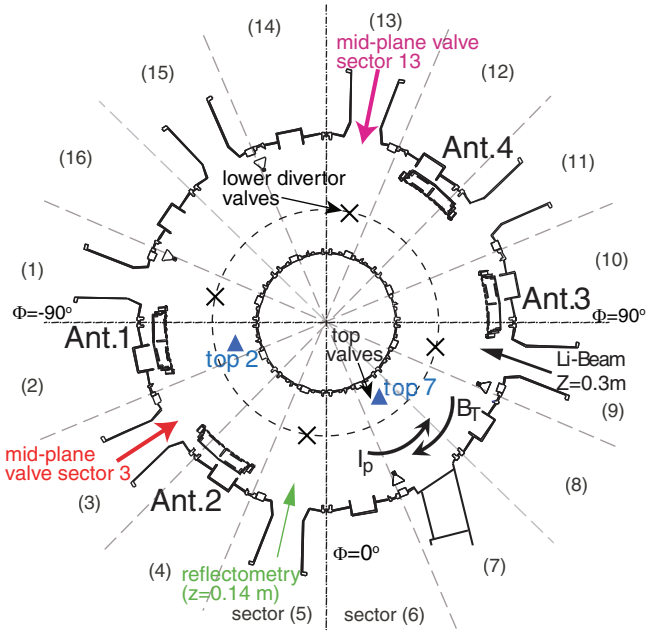

Figure 3. Top view of AUG illustrates the toroidal positions of the ICRF antennas and gas valves.

The density (n_e) and temperature (T_e) profiles in the mid-plane and the ion saturation current density (j_{sat}) in the divertor are fitted to the experiments by modifying the transport parameters (i. e. particle and heat diffusion coefficient $D_\perp$ and $\chi_\perp$, respectively) in the code. The diagnostics used in the comparisons include the Lithum beam for n_e [17], the edge and core Thomson scattering for n_e and T_e [18], and the divertor Langmuir probes for j_{sat} [19]. Only the inter-ELM experimental data is used, because the inter-ELM phases are those of interest corresponding to the lowest coupling resistance and maximum antenna voltages [8]. The transport parameters are chosen such that the final n_e, T_e and j_{sat} profiles in our simulations agree well with the experiments (figure 4), except for the j_{sat} values at the inner strike point.

In the simulation setups for the lower divertor gas puff, the upstream and downstream profiles in the SOL are best matched to the experiments via choosing the proper particle and energy transport parameters $D_\perp$ and $\chi_\perp$. To illustrate the sensitivities of the chosen transport parameters on the simulated results, density scans are made via changing the particle transport parameters $D_\perp$ for ρ_{pol} in the range [1.03, 1.1] (a range where the FW cut-off layer is located). As $D_\perp$ varies in the range [0.6, 1.5 m^2 s^{-1}], the density profiles in the far SOL only change in a level lower than 10%, and the FW cut-off layer is shifted within 0.3 cm (less than 10% of the FW evanescent distance). The changes of the density near the FW cut-off layer have negligible impact on the antenna coupling. Moreover, by comparing the relative improvement of the coupling resistance R_c (figure 8), the error of the calculated R_c due to the uncertainties of the transport parameters is minimized.

After validating our simulations with experiments for the lower divertor gas puff case, the gas sources are then switched to the top or the outer mid-plane of the vessel to study the related changes in the 3D distribution of n_e and T_e. For experiments in AUG, usually 4 gas valves are used for the lower divertor gas puff, and one for each top or outer mid-plane gas puff. The following cases (table 2) were simulated in parallel with the experiments (table 1): I. four lower divertor gas valves in sectors 1, 5, 9, 13 (toroidal angle $\Phi = -101.25°$, $-11.25°$, $78.75°$, $168.75°$); II. one top gas valve in sector 2 ($\Phi = -78.75°$); III. one top gas valve in sector 7 ($\Phi = 33.75°$); IV. one outer mid-plane gas valve in sector 3 ($\Phi = -56.25°$); V. one outer mid-plane gas valve in sector 13

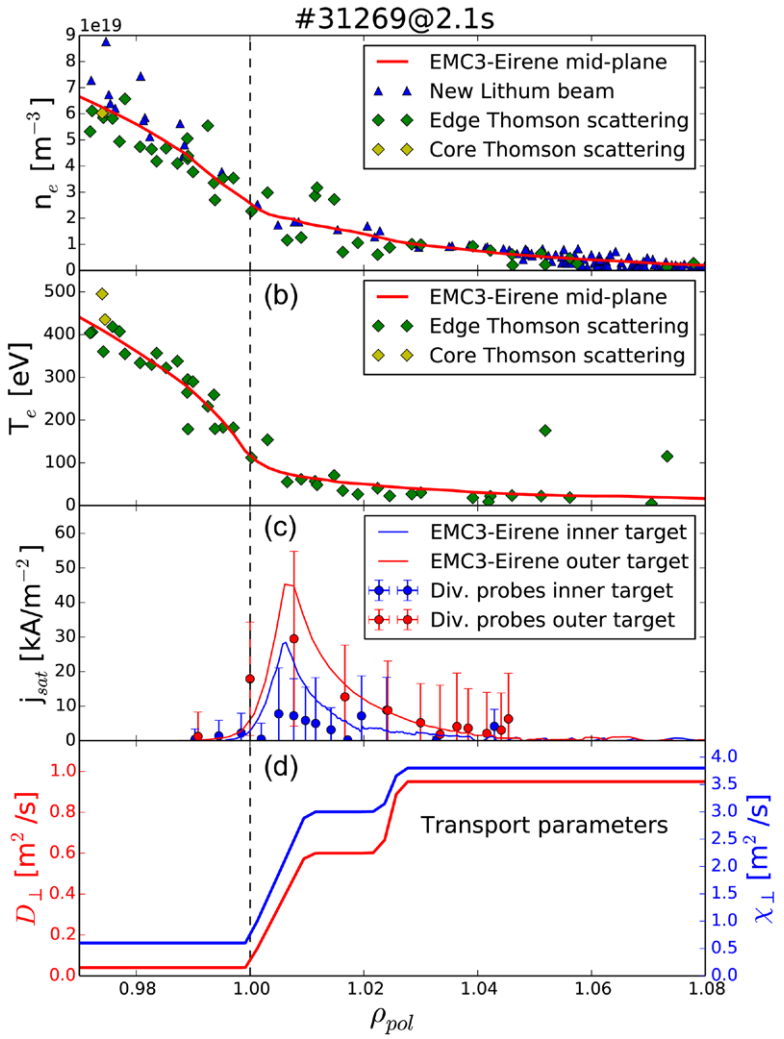

Figure 4. EMC3-Eirene simulations compared with experimental diagnostics for the lower divertor gas puff (case I). (*a*) Comparisons of mid-plane density profile. (*b*) Comparisons of mid-plane temperature profile. (*c*) Comparisons of the ion saturation current density in the targets. (*d*) Transport parameters $D_\perp$ and $\chi_\perp$ in the code.

Table 2. The simulated cases in parallel with the experiments.

Simulated cases	Valve positions (toroidal)	Gas puff rate
Case I (lower divertor puff)	Sector 1 ($\Phi = -101.25°$), sector 5 ($-11.25°$) Sector 9 (78.75°), sector 13 (168.75°)	0.3×10^{22} el s^{-1} for each valve
Case II (A02 top puff)	Sector 2 ($\Phi = -78.75°$)	1.2×10^{22} el s^{-1}
Case III (A07 top puff)	Sector 7 ($\Phi = 33.75°$)	1.2×10^{22} el s^{-1}
Case IV (A03 outer mid-plane puff)	Sector 3($\Phi = -56.25°$)	1.2×10^{22} el s^{-1}
Case V (A13 outer mid-plane puff)	Sector 13 ($\Phi = 168.75-$)	1.2×10^{22} el s^{-1}

($\Phi = 168.75°$). The total gas puff rate in all cases is the same (1.2×10^{22} el s^{-1}).

3. Simulation results

3.1. Gas puff effects on edge density

Poloidal cross-sections of the neutral atom densities during the lower divertor, the top and the outer mid-plane gas puff are shown in the upper row of figure 5. Toroidal positions are chosen where the gas valves are placed, so the poloidal cross-sections are the same either for the top gas puff case II ($\Phi = -78.75°$) and case III (($\Phi = 33.75°$), or for the outer mid-plane gas puff case IV ($\Phi = -56.25°$) and case V (($\Phi = 168.75°$). The arrows in the figure are used to represent the positions and directions of the injected gas. A localized cloud of neutrals near the valves could be seen both in the top and the lower divertor gas puff cases. For the outer mid-plane gas puff, the poloidal and toroidal distribution of the enhanced neutral density essentially corresponds to the shape of the

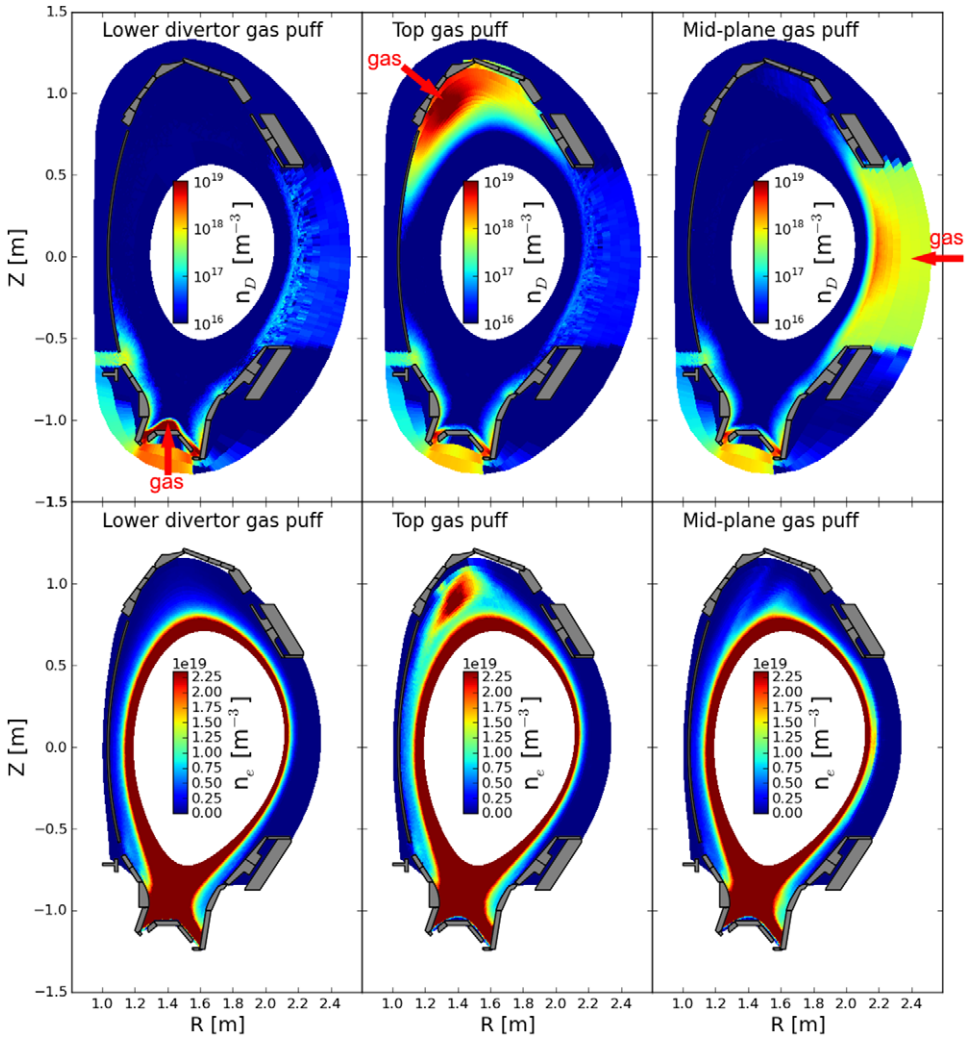

Figure 5. Poloidal cross sections of the neutral atom and electron densities for the lower divertor, top and outer mid-plane gas puff cases. In all cases the gas puff rate is the same. The cross-sections are the same either for the top gas puff case II ($\Phi = -78.75°$) and case III ($\Phi = 33.75°$), or for the outer mid-plane gas puff case IV ($\Phi = -56.25°$) and case V ($\Phi = 168.75°$).

so-called A-port. The corresponding electron densities are depicted in the lower row of figure 5. The radial and poloidal localization of the electron density near the top gas valve (figure 5, second column) can be explained by the fact that the gas is ionized locally in the SOL and the particle transport in the parallel direction of the magnetic field is much larger than in the perpendicular. For the outer mid-plane gas puff, the density is enhanced in a large poloidal range in the outer mid-plane. The striped density structures in the top of the SOL are consequences of helical paths in which magnetic field lines connect the mid-plane and top (figure 5, third column).

Note that the outer mid-plane gas valves are located very deep in the A-port in AUG. Before the gas reaches the plasma edge, it has already spread widely and becomes an almost homogeneous source in the cross-section of the port. The scattered gas is firstly shaped by the front face of the port and then by the PFCs such as the limiters. In the simulations, we have put the mid-plane gas valves as far as possible to the edge of the computational grid. In that way the gas fills-up the A-port. This gives a realistic description of the ionization area where

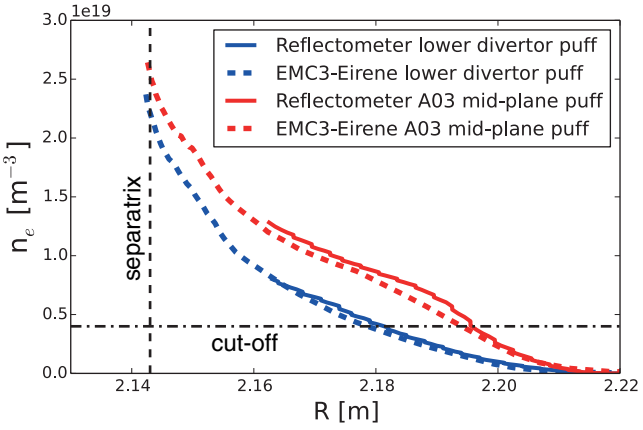

Figure 6. Density comparisons with the reflectometer measurement in sector 5 for the lower divertor gas puff (case I) and the A03 mid-plane gas puff (case IV). The reflectometer profiles (#30634) are averaged over time period 2.1–2.3 s (the lower divertor puff) and 5.9–6.1 s (the A03 mid-plane puff) respectively. Only the inter-ELM reflectometer data is used.

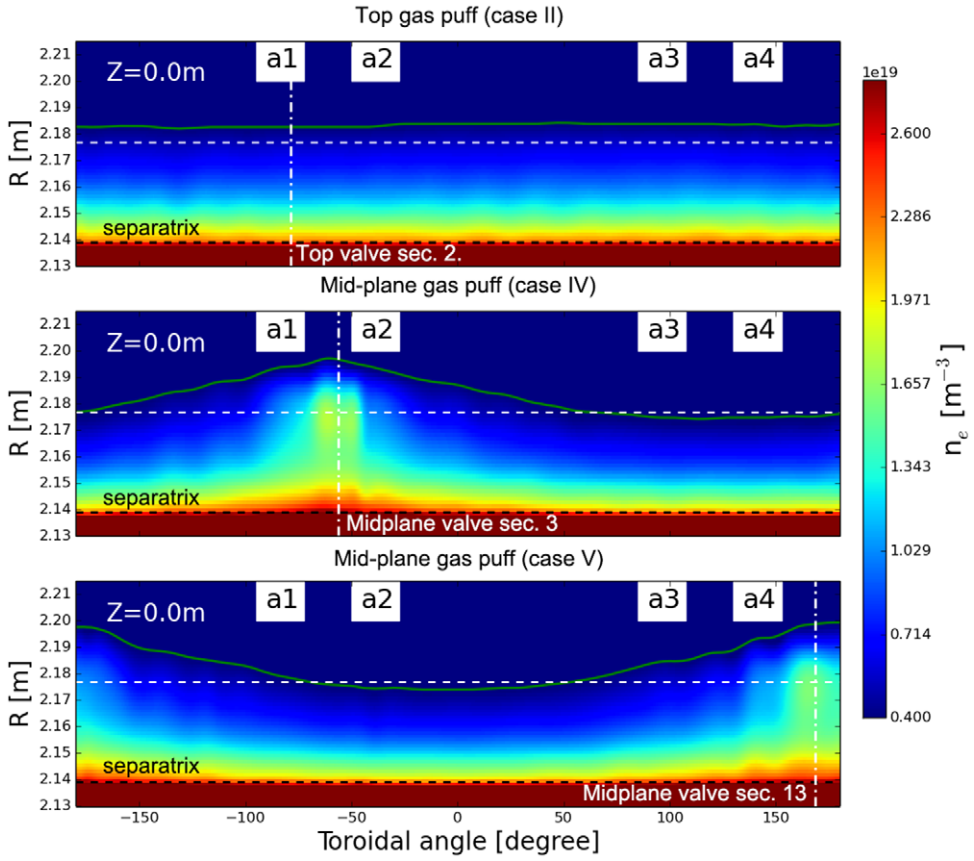

Figure 7. Toroidal cross sections (at $Z = 0.0$ m) of the electron density for cases II, IV and V. In each subplot, the green line represents the position of the cut-off density, while the horizontal dashed line represents this position for case I. The vertical dash-dotted line means the toroidal angle of the gas valve.

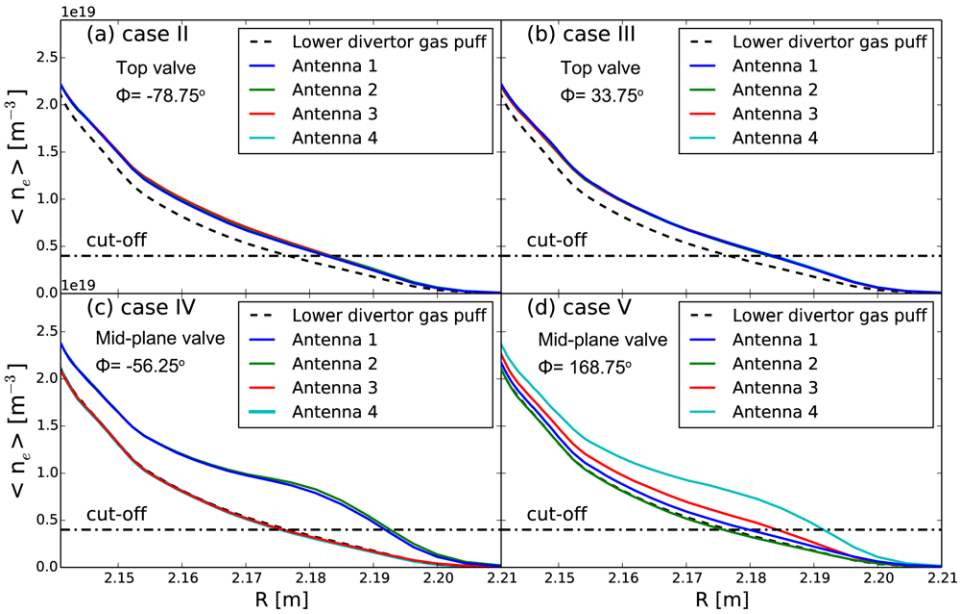

Figure 8. Comparisions of the averaged densities in front of the four antennas for the top gas puff (case II, III) and the outer mid-plane gas puff (case IV, IV). In each subplot, the dashed line represents the density profile in the lower divertor gas puff (case I).

neutrals interact with the plasma. Figure 6 shows the electron density comparisons between the EMC3-Eirene simulations and reflectometer measurement in sector 5 (~1.73 m away from the A03 mid-plane valve, figure 3). For the reflectometer data (#30634), only densities in the range [0.3×10^{19}, 1.5×10^{19} m^{-3}] are accurate, and those below 0.3×10^{19} m^{-3} are extrapolated. Good agreement is found for the lower divertor gas puff (case I), while only a small discrepancy in the density range [0.4×10^{19}, 0.85×10^{19} m^{-3}] is seen for the A03 mid-plane gas puff (case IV). This shows that the

physical description of the outer mid-plane valve in EMC3-Eirene is reasonable.

To investigate the edge density distributions in the toroidal direction, toroidal cross-sections in the outer mid-plane ($Z = 0.0$ m) are made for the cases I, II, IV and V (figure 7). Only densities larger than the cut-off density (~4×10^{18} m^{-3}) are shown in the plot. The position of the cut-off density for case I (the horizontal dashed line) is used as a reference. The results indicate that the edge density is increased toroidal uniformly by a small margin with the top gas puff, while the density near the valves can be notably increased with the outer mid-plane gas puff. This density increase significantly reduces the width of the evanescent layer. For the density in the region far away from the outer mid-plane valve, no obvious change can be seen.

Furthermore, we calculated the averaged electron density in front of each ICRF antenna. This average is made both in the poloidal and toroidal directions covering the whole range of the antenna, namely

$$\langle n_e(\psi)\rangle = \frac{1}{\Delta\theta\Delta\Phi}\int_{\theta_0-\Delta\theta/2}^{\theta_0+\Delta\theta/2}\int_{\Phi_0-\Delta\Phi/2}^{\Phi_0+\Delta\Phi/2} n_e(\psi,\theta,\Phi)\mathrm{d}\theta\mathrm{d}\Phi$$

in which θ_0 and Φ_0 represent the poloidal and toroidal angles of the antenna center, and $\Delta\theta$ and $\Delta\Phi$ are the angles between the edges of the antennas in the poloidal and toroidal directions respectively. The averaged density in each flux surface $\langle n_e(\psi)\rangle$ is then transformed to $\langle n_e(R)\rangle$ at $Z = 0.0$ m. The results are shown in figure 8. In each subplot, the dashed line represents the averaged density profile during the lower divertor gas puff (case I), and the dash-dotted lines is the cut-off density of the ICRF FW. From the analysis we find that the top gas puff can increase the edge density only to a small extent. However, this increase is toroidally uniform and independent of the toroidal positions of the gas valve (figures 8(*a*) and (*b*)). The outer mid-plane gas puff can significantly increase the edge density in the area near the valve. In the case IV, the gas valve is located between antenna 1 and 2 (closer to antenna 2) and far away from antenna 3 and 4, thus the density is enhanced largely in front of antennas 1 and 2, while almost no change is observed for antennas 3 and 4 (figure 8(*c*)). In the case V, the toroidal distance from the valve to the antennas 4, 3, 1, 2 is increasing, and the density enhancement has the inverse trend, i.e. the largest density increase is seen for antenna 4 and the smallest for antenna 2 (figure 8(*d*)). The top gas puff (cases II or III) can reduce the evanescence distance by ~0.73 cm, while the outer mid-plane gas puff can have a larger effect, such as case IV can make this distance smaller by ~1.96 cm. Based on these results and further calculations with FELICE [20], the coupling resistances can be calculated.

3.2. Gas puff effects on ICRF power coupling

As mentioned in the introduction, the coupled ICRF power is proportional to the coupling resistance R_c, while R_c is exponentially to the evanescent distance d_{evan}. Comparing to the lower divertor gas puff, the top or outer mid-plane gas puff substantially increase the edge density. As a result, the width of the evanescent layer for the FWs is decreased and the ICRF

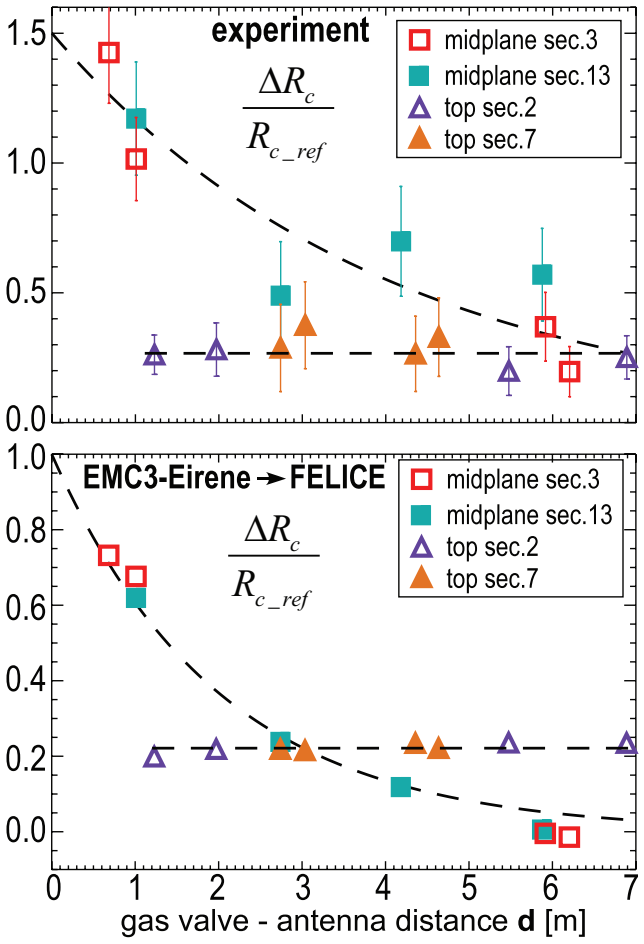

Figure 9. The relative improvement of antenna coupling resistance $\Delta R_c/R_{c\_ref}$ as a function of gas valve-antenna distance.

power coupling is improved. In experiments, R_c is estimated from the measurements of RF voltage and power by RF detectors. Figure 9 shows the relative change of the coupling resistance, $\Delta R_c/R_{c\_ref}$, with the distance between valves and antennas, where R_{c_ref} is the resistance for the lower divertor gas puff (case I). We use this as reference value, since the lower divertor gas puffing results in almost the same and lowest coupling resistance for all the antennas [21]. This behaviour can be explained by the toroidally uniform density and the largest FW evanescent distance during lower divertor gas puffing (figure 7). In simulations, the coupling resistance is calculated by using the density profile from EMC3-Eirene in the antenna FELICE code [20]. FELICE solves the Maxwell equations in a hot plasma to estimate the plasma surface impedance [22] and the antennas are approximated with thin straps parallel to the plasma boundary and to the wall. In FELICE code the plasma is assumed plane-stratified with the confining magnetic field in the toroidal direction and the plasma parameters varying only in the radial direction [20]. As a consequence, the 3D edge density and temperature profiles calculated with EMC3-Eirene must be firstly averaged into 1D for each antenna and, then, matched with the corresponding experimental core profiles. In this way, inputs are provided to the FELICE code, which, in turn, calculates the coupling resistance. Figure 9(*b*) shows the variation of the coupling resistance calculated with

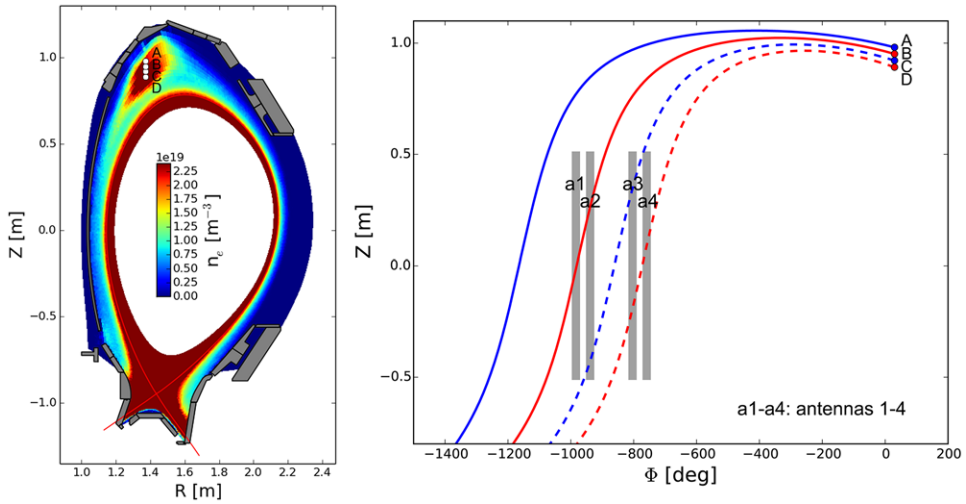

Figure 10. Field lines tracing from the top. The starting points A, B, C, D (in a vertical line) are within the plasma density cloud in front of the top valve.

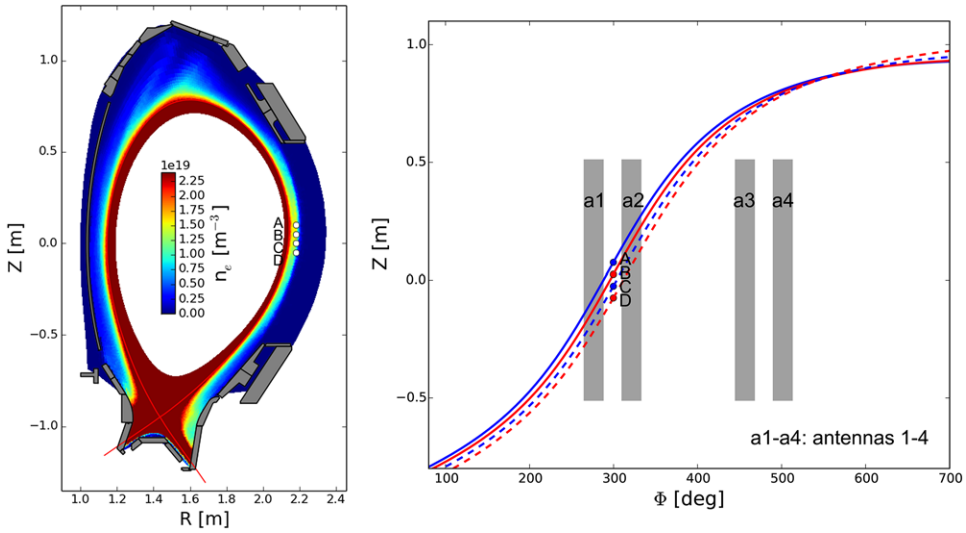

Figure 11. Field lines tracing from the outer mid-plane. The starting points A, B, C, D (in a vertical line) are within the plasma density cloud in front of the outer mid-plane valve.

EMC3-Eirene and FELICE codes in the same way of the experimental values shown in figure 9(*a*).

From both the experimental measurements (figure 9(*a*)) and simulation results (figure 9(*b*)), we observe that the top gas puff can improve the coupling resistance by 20% ~ 30%, and this improvement is even higher for the outer mid-plane gas puff, especially for antennas near the gas valves. Indeed, a coupling improvement of more than 100% with the outer mid-plane gas puff is observed in experiments for antenna 1 and 2 during A03 puffing (case IV) and for antenna 4 during A13 puffing (case V). The EMC3-Eirene and FELICE results agree well with measurements for the top gas puff (case II and III). However, for the outer mid-plane gas puff (case VI and V), although the correct trend is reproduced by simulations, the calculated values are consistently lower than the measurements with an offset of about 0.4. Various mechanisms can be responsible for the larger off-set observed for the outer mid-plane gas puff cases:

1. By averaging the 3D edge profiles of EMC3-Eirene we neglect poloidal and toroidal inhomogeneity of the density in front of the antennas, consequently inaccuracies can be introduced. As an example, if we consider A03 mid-plane puff (case IV), the 1D density profile (figure 8) shows the cut-off density layer is at $R = 2.193$ m for antenna 2. However, for the toroidal cross section of the density profile (figure 7) one can infer that this cut-off position varies in the range [2.189 m, 2.196 m] for the same antenna. This variation can be even larger along the poloidal direction. For the top gas puff, because the density is enhanced toroidal uniformly, thus the averaging does not have much effect.
2. In this study, we have not addressed the complex problem of the impact of the parasitic RF effect [26] on the ionization rate of the neutrals in the plasma edge. As an order of magnitude, in the next section we estimate the energy and the density that the fast electron population generated

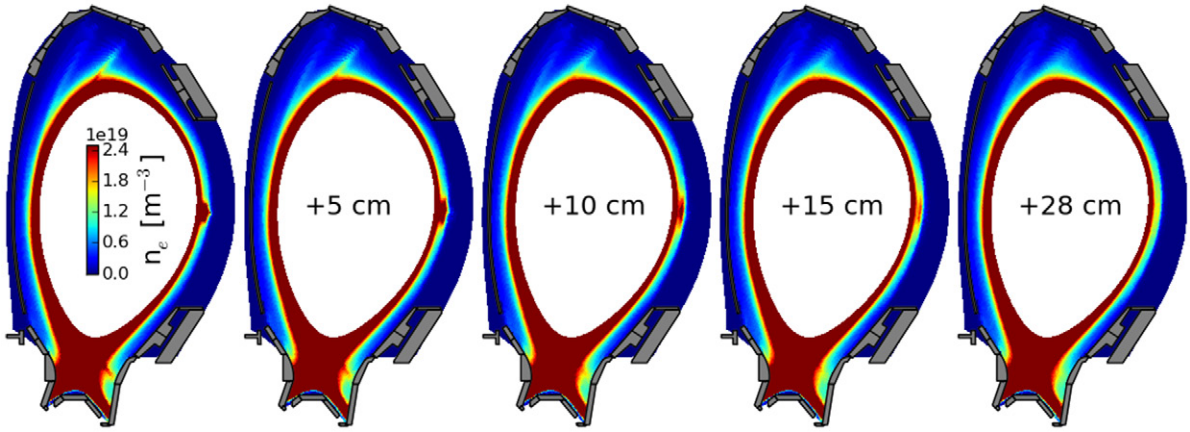

Figure 12. Variations of the 2D density profiles when radially shifting the outer mid-plane gas valve outward.

by parasitic RF effects should have to substantially affect the ionization rate. A more quantitative estimate of this effect is out of the aim of the present study, and it is left for the future. Moreover, large inhomogeneous rectified potentials and ponderomotive effects can be induced in front of antennas, resulting in significant convective transport in the plasma edge [23, 24]. This convective transport will cause local density modifications and ultimately influence the coupling resistance.

3. The ELMs change the SOL properties. Although we have been filtered out the time window of each ELM event, residual effects might be still play a role in our analysis.

Measurements clearly show that the outer mid-plane gas valves are the most effective in improving antenna coupling. And in turn, EMC3-Eirene&FELICE simulations explain this finding with a substantial change of the SOL density near the antennas. However, for improving the quantitative agreement with measurements and therefore their predictive capabilities, several improvements of our simulations have to be undertaken in the near future by addressing the aforementioned issues.

4. Mechanisms of influence of local gas puff on density in the SOL

Different gas puff methods, i.e. gas puffing from the top, outer mid-plane or bottom (the lower divertor) of the machine, can lead to different edge density profiles and ICRF power coupling resistances. Our studies indicate that this is mainly due to the magnetic connections to the ion density cloud in front of the gas valves. A cloud of neutrals puffed at the plasma edge leads to the formation of a plasma density cloud due to ionization (figure 5). The ionization rate of the neutrals by electron impact can be calculated with the formula $S_{\mathrm{p,iz}} = n_{\mathrm{e}} n_{\mathrm{n}} \overline{\sigma\nu}_{\mathrm{iz}}(T_{\mathrm{e}})$ [25], where n_{e} is the plasma density and n_{n} is the neutral density. The rate coefficient $\overline{\sigma\nu}_{\mathrm{iz}}(T_{\mathrm{e}})$ only depends on the electron temperature T_{e}. For the gas cloud (figure 5) formed in the top or outer mid-plane (inside the main chamber wall) of the machine, the electron temperature is quantitative above the threshold temperature (~2 eV) for ionization. The ionized particles in the gas cloud will strongly follow the magnetic field lines, since from the fluid plasma consideration, the velocities parallel to the magnetic field lines are much larger than the crossing field ones. Thus on the same flux surface, electron densities in the regions which are magnetically connected to the plasma density cloud can be higher than those without.

This is shown by tracing the magnetic field lines from the plasma density cloud in front of the valves (figures 10 and 11). Four vertical points within the cloud are chosen for the field line tracings. For the top gas puff, field lines encounter a large toroidal spread from the top toward the outer-mid-plane which explains the evenly toroidally distributed density at the outer mid-plane (figure 10). For the outer mid-plane gas puff, field lines start from the mid-plane have little divergence in a large toroidal range [200°, 400°] when they travel to the top or bottom of the machine (figure 11). The magnetic field lines penetrating the plasma density cloud would also pass in front of antennas 1 and 2, resulting in significantly increased electron density there. Thus, gas valves which can generate a homogenous density cloud covering the height of the antennas and being magnetically connected to the antennas are preferred.

It is important to note that the toroidal and poloidal localization of the ionization is determined by the position of the gas puff. The radial localization of the gas puff is determined by the combination of electron temperature, electron density and neutral density calculated self consistently by EMC3-EIRENE. In the present of powered ICRF antennas, the RF fields can generate fast electrons which may hit the gas cloud and cause additional ionization. This ionization exist either in the region near the antennas where electrons gain energy from the slow wave, or in the region far from the antennas where electrons gain energy from the ponderomotive force [26, 27]. To calculate the effect of a population of fast electrons, profiles of T_{e}, n_{e} and n_{D0} from the EMC3-EIRENE calculations at the position of the gas puff were used. The ionization rate of D0 to D+ assuming the existence of a local population of fast electrons with a temperature of 100 eV and a relative density of α times the electron density from EMC3-EIRENE, together with the ionization rate of 1-α times the rate expected from

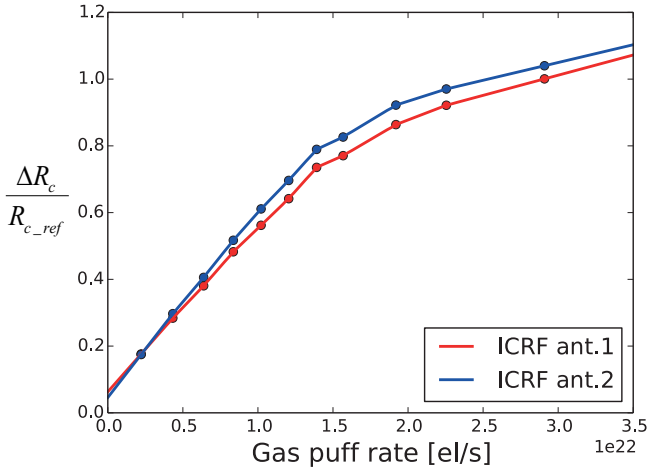

Figure 13. The simulated relative resistance as a function of gas puff rate for a typical H-mode discharge (#31269).

the EMC3-EIRENE profiles were calculated using ADAS rates. At the position of peak ionization rate with $\alpha = 0$, the increases in ionization rate for $\alpha = 0.001$, 0.01 and 0.1 were 0.2%, 2% and 20%, respectively. While such a linearized calculation is an approximation, it is expected that is should be reasonably accurate for α less than or equal to 0.01. Efforts are underway to calculate the wave electric fields in the region of the gas puff, and these could then be used to estimate the energy and density of a fast electron population. If these turn out to be significant, then the effects of these fast electrons could be included in future EMC3-EIRENE simulations.

5. Strategies for gas puff optimization

Gas puffing at the outer mid-plane of the vessel is indicated to be the most effective in improving the ICRF coupling. When applying this method, one needs to consider the particle and power fluxes to the main chamber wall. As shown in figure 12, if the outer mid-plane gas valve is put too close to the limiter, a large density bump would occur in the plasma edge. This can cause significant particle flows to the PFCs and large amounts of impurities might be sputtered. The density bump can be eliminated by radially shifting the gas valve outward. The more radially retracted the gas valve is, the more poloidally homogenous the electron density would be. During the shifting process (figure 12), the coupling is found not decreased as long as the plasma density cloud is within the height of the antennas. To generate a homogenous density cloud covering the antenna, one can also use poloidally distributed gas valves. For example in AUG, 11 poloidally distributed gas valves behind the left limiter of antenna 3 are being installed to improve the coupling of the nearby antennas.

Besides the valve positions, the gas puff rate Φ_{D2} has also an important impact on the coupling. To understand the relationship between Φ_{D2} and the coupling, simulations are carried out for the A03 mid-plane gas puff (case IV) with different Φ_{D2}. Combined EMC3-Eirene and FELICE simulations are used to calculate the relative improvement of coupling resistance $\Delta R_c/R_{c\_ref}$. The results (figure 13) indicate that $\Delta R_c/R_{c\_ref}$ could be increased simply by increasing Φ_{D2}. However this does not mean that the higher Φ_{D2} the better, since a strong gas puff can degrade the plasma confinement [28]. In addition, the relative increase of R_c/R_{c0} would become smaller when Φ_{D2} is larger. For instance R_c/R_{c0} increases almost linearly for Φ_{D2} in the range $A = [0, 1.5 \times 10^{22}$ el s$^{-1}]$ and $B = [1.9 \times 10^{22}$, 3.5×10^{22} el s$^{-1}]$, but the slope of Φ_{D2} in the range A (k_A) is much larger than the one in the range B (k_B). For antenna 1, k_A ~0.478, k_B ~0.138, and for antenna 2, k_A ~0.526, k_B ~0.119. From the economical view, gas puffing with Φ_{D2} in the range $[1.2 \times 10^{22}$, 1.9×10^{22} el s$^{-1}]$ can achieve a high coupling resistance most effectively.

6. Conclusions and outlooks

For the first time EMC3-Eirene simulations for AUG with a full 360° grid including the main chamber PFCs, divertors and 3D gas puffs were carried out. Our simulation results are in qualitative agreement with the experiment: The top gas puff can increase the edge density uniformly in toroidal direction to a small extent, independent of the toroidal position of the top valves; for the outer mid-plane gas puff the enhancement of the edge density is most significant near the valve and gradually decreases away from the valve in the toroidal direction. The outer mid-plane gas puff is most efficient in increasing the ICRP coupling for the antennas nearby, while the top gas puff increases the coupling for all the antennas in a significant smaller degree. Our study indicates that the connection between the cloud of enhanced plasma density and the antennas along magnetic field lines is the reason for the density enhancement in front of the antennas. The plasma density cloud is generated from the ionization of the injected gas near the valves. Thus for ICRF coupling purposes, if poloidal localization of the density increase is not problematic, poloidally distributed gas valves (covering the height of the antennas) which are close to the ICRF antennas in the toroidal direction is the better option.

In the near future we will have better comparison with experiments as more toroidal distributed reflectometers are being installed in AUG. Further EMC3-Eirene simulations and comparisons with experiments in L and H mode discharges in AUG will allow optimization of the gas valve positions in AUG for the purpose of ICRF power coupling and reliable benchmarking of the 3D code in view of its use for ITER. We plan to carry out similar simulations for JET and ITER including the divertor/PFCs/gas valves configurations in full 360° geometry.

Acknowledgments

This work has been carried out within the framework of the EUROfusion Consortium and has received funding from the Euratom research and training programme 2014–2018 under grant agreement No 633053. The views and opinions expressed herein do not necessarily reflect those of the European Commission.

References

[1] Bilato R. *et al* 2005 *Nucl. Fusion* **45** L5–7
[2] Jacquet P. *et al* 2012 *Nucl. Fusion* **52** 042002
[3] Bobkov V. *et al* 2014 *AIP Conf. Proc.* **1580** 271
[4] Lerche E. *et al* 2014 *J. Nucl. Mater.* **463** 634–9
[5] Mayoral M.-L. *et al* 2007 *AIP Conf Proc.* **933** 55
[6] Pinsker R.I. *et al* 2011 *37th EPS Conf.* http://ocs.ciemat.es/EPS2010PAP/pdf/O4.124.pdf
[7] Pinsker R.I. *et al* 2011 *AIP Conf Proc.* **1406** 313
[8] Jacquet P. *et al* 2014 *Proc. 25th Int. Conf. on Fusion Energy* (*St. Petersburg, Russia*) EX/P5-39
[9] Feng Y. *et al* 2004 *Contrib. Plasma Phys.* **44** 57–69
[10] Reiter D. *et al* 2005 *Fusion Sci. Technol.* **47** 172–86
[11] Feng Y. *et al* 2014 *Contrib. Plasma Phys.* **54** 426–31
[12] Frerichs H. *et al* 2010 *Nucl. Fusion* **50** 034004
[13] Lunt T. *et al* 2012 *Nucl. Fusion* **52** 054013
[14] Zhang W. *et al* 2015 *21st RF Topical Conf. RF Power in Plasmas (Los Angeles, USA)* p A56
[15] Lunt T. *et al* 2015 *J. Nucl. Mater.* **463** 744–7
[16] McCarthy P.J. 1999 *Phys. Plasmas* **6** 3554
[17] Fischer R. *et al* 2008 *Plasma Phys. Control. Fusion* **50** 085009
[18] Kurzan B. *et al* 2011 *Rev. Sci. Instrum.* **82** 103501
[19] Weinlich M. *et al* 1996 *Contrib. Plasma Phys.* **36** 53–60
[20] Brambilla M. *et al* 1989 *Plasma Phys. Control. Fusion* **31** 723
[21] Bobkov V. *et al* 2015 *21st RF Topical Conf. RF Power in Plasmas (Los Angeles, USA)* p A44
[22] Brambilla M. *et al* 1995 *Nucl. Fusion* **35** 1265–80
[23] Colas L. *et al* 2007 *Plasma Phys. Control. Fusion* **49** B35–45
[24] Eester D.-V. *et al* 2013 *Plasma Phys. Control. Fusion* **55** 025002
[25] Stangeby P.C. 2000 *The Plasma Boundary of Magnetic Fusion Devices* (London: Taylor & Francis)
[26] Tripský M. *et al* 2014 *41st EPS Conf. on Plasma Physics (Berlin, Germany)* P1.133
[27] Lyssoivan A. *et al* 2012 *Plasma Phys. Control. Fusion* **54** 074014
[28] Kalupin D. *et al* 2001 *Plasma Phys. Control. Fusion* **43** 945–57